THE ASTROPHYSICAL JOURNAL, 408:471–483, 1993 May 10

INFRARED IMAGES OF THE YOUNG CLUSTER NGC 2264

CHARLES J. LADA
Harvard-Smithsonian Center for Astrophysics, 60 Garden Street, Cambridge, MA 02138; and Steward Observatory, University of Arizona
ERICK T. YOUNG
Steward Observatory, University of Arizona, Tucson, AZ 85721
AND
THOMAS P. GREENE
Institute for Astronomy, University of Hawaii, 2680 Woodland Drive, Honolulu, HI 96822
Received 1992 August 3; accepted 1992 November 10

ABSTRACT

We present the initial results of an extensive infrared imaging survey of the young cluster NGC 2264 and a nearby galactic control field. A large portion of the cluster was imaged in each of the three standard near-infrared colors (J, H, and K) with an infrared array camera. Similar observations were obtained of a large nearby region off the cluster and its associated molecular cloud. Comparison of these observations enabled us to estimate the size of the cluster population and investigate the nature of its members. In the region of the cluster surveyed at 2.2 μm (K), we detected more than 1,650 sources. After correcting for background/foreground field stars we find that the cluster contains 360 ($\pm$ 130) members. We find that the slope of the K luminosity function of the cluster is significantly steeper than that expected for a cluster of ZAMS stars and appears to flatten out or turn over at an apparent K magnitude of roughly 13.0–14.0. Both the slope and the turnover in the luminosity function can be modeled with an underlying cluster mass function which is similar to the Miller-Scalo or local field star IMF, provided that a mass-luminosity relation appropriate for pre–main-sequence stars applies to the cluster population. From analysis of the JHK color-color diagrams of the cluster and control fields we find that approximately 170 sources observed toward the cluster have colors indicative of intrinsic excess infrared emission. Consequently, infrared excess stars appear to account for a relatively large fraction (50% $\pm$ 20%) of the cluster membership. These stars have near-infrared colors similar to those of young emission-line stars such as classical T Tauri stars and Herbig AeBe stars. Circumstellar disk models can account for the colors of most of these sources. That circumstellar disks are inferred for such a large fraction of the cluster membership argues for disk lifetimes which are at least as long as the age of the cluster (i.e., 5×10^6 yr). Many of these stars are also characterized by relatively large amounts of extinction and may be partially embedded in the molecular cloud behind the cluster.

Subject headings: infrared: stars — open clusters and associations: individual (NGC 2264) — stars: formation

1. INTRODUCTION

Young galactic clusters which are embedded in or intimately associated with molecular clouds provide important laboratories for the study of the early phases of stellar evolution and star formation. This is primarily because such clusters contain statistically significant samples of young stellar objects (YSOs) of the same parental heritage but of differing mass and evolutionary states. The close proximity of cluster members enables direct observation and comparison of their physical natures. Renewed interest in observations of extremely young clusters has been sparked by two recent developments. First, a detailed infrared imaging survey of the L1630 (Orion B) giant molecular cloud has shown that star formation activity for both low- and high-mass stars in that cloud has occurred almost exclusively within a few (three) rich embedded clusters (E. Lada et al. 1991). If L1630 is in any way typical of GMCs in the galaxy, then a larger fraction of galactic star formation may have occurred within young embedded clusters than has previously been supposed. Second, the development of large-format infrared array cameras has enabled the simultaneous and near-simultaneous multiwavelength observation of relatively large regions of sky, making it realistically possible to obtain multicolor near-infrared observations for entire clusters and embedded stellar populations in molecular clouds in reasonable amounts of time (e.g., C. Lada et al. 1991; Gatley et al. 1991; Barsony, Shombert, & Kis Halas 1991; Greene & Young 1992; Eiroa & Casali 1992; Carpenter et al. 1993). Moreover, a recent analysis by Lada & Adams (1992) has demonstrated the potential usefulness of such multicolor infrared observations for statistical investigation of the physical natures of large groups of YSOs.

In this paper we present the first results of an extensive near-infrared imaging survey we undertook of the young cluster NGC 2264. The early pioneering observations of Herbig (1954), Walker (1956), Warner, Strom, & Strom (1977, hereafter WS[2]), and Blitz (1979) along with the more recent work of Adams, Strom, & Strom (1983, hereafter AS[2]), Margulis, Lada, & Young (1989, hereafter MLY), Margulis, Lada, & Snell (1988) and others have established this region as an important laboratory for studies of star formation and pre–main-sequence stellar evolution. In particular, Herbig (1954) discovered Hα emission-line stars in the cluster which were subsequently shown by Walker's (1956) photometric measurements to be pre–main-sequence (PMS) in nature. Indeed, Walker's observations suggested that nearly all the stars in the cluster with spectral types later than A0 lie above the main sequence. This resulted in an age estimate of roughly 5×10^6 yr for the cluster. The early infrared observations of Strom,

Strom, & Yost (1971) and WS[2] suggested that many, perhaps a third, of the PMS stars in the cluster were characterized by infrared excess emission and consequently associated with circumstellar material of one form or another. Blitz (1979) showed that the cluster lies in front of a massive GMC whose effective extinction of background field stars was originally noted by Herbig (1954). The observations of Margulis & Lada (1986), Margulis et al. (1988), and MLY further established that the molecular cloud behind the cluster is still an active site of star formation containing numerous molecular outflows and discrete, presumably embedded, *IRAS* sources.

We undertook the extensive infrared imaging survey reported here in order to significantly expand the existing data base of infrared observations of this important cluster. The primary goals of our study were to obtain a census of the cluster population, to investigate its infrared luminosity function, to obtain a more complete determination of the number of infrared excess stars in the cluster, and to provide an extensive data base of observations which could be of (future) use for investigating the variability of YSOs at infrared wavelengths. In addition, such extensive infrared observations could ultimately be useful for the construction of the star formation history of the complex and the elucidation of the relation between the cluster and molecular cloud. In § 2 we describe our instrumentation, data collection methods, and initial image reduction procedures. In § 3 we explain the methods we used for extracting sources, obtaining photometry, and determining the astrometry of our data set. In § 4 we present the basic results of our observations, and in § 5 we discuss their implications. The main conclusions of this work are summarized in § 6.

2. INSTRUMENTATION AND OBSERVATIONS

2.1. *NICMOS–Steward Observatory*

Our near-infrared imaging survey of the young cluster NGC 2264 was made with the Steward Observatory 128 × 128 HgCdTe NICMOS array camera developed by Rieke et al. (1989) and for this project attached to the University of Arizona Observatories 1.55 m (61 inch) telescope located on Mount Bigelow outside Tucson, Arizona. Images were obtained in three standard infrared colors: J (1.25 μm), H (1.65 μm), and K (2.2 μm) during three separate observing sessions. The J and H observations were obtained during 1990 March and 1990 January, respectively. For these observations the optics were configured to provide a coarse pixel scale (1.″78 pixel^{-1}) and thus enabled us to image a relatively large region of the sky with extensive overlapping of frames. The J-band survey consisted of 110 individual images which were arranged in a 10 column by 11 row mosaic roughly 21′ × 38′ on a side covering an area of about 800 arcmin^2. The individual images were overlapped by approximately 2′ ($\frac{1}{2}$ frame width) in right ascension and 35″ in declination. The extensive overlapping of the images enabled an accurate positional mosaic of the region to be constructed and provided redundancy for the photometric observations of objects in the region. The H-band survey also consisted of 110 individual images positioned in a grid similar to those in the J mosaic. The K band observations were obtained in 1991 November with a finer pixel scale (0.″9 pixel^{-1}), and images in the K mosaic were overlapped by 1′ ($\frac{1}{2}$ frame size) in both right ascension and declination. A total of 450 frames were taken in a 15 × 30 grid. As a result the K-band survey covers a smaller area on the sky, roughly 540 arcmin^2. The integration times were 40 s at J, 36 s at H, and 40 s at K.

First-order corrections for sky and telescope emission were made by subtracting from the frame in question a median of all the frames in the same row. We have found this method to be more efficient than explicitly observing sky frames, and it better avoids potential problems with sources in the off frame. Gain variations over the array were corrected by dividing the image with a dark-subtracted, normalized composite sky frame.

In the course of our reductions, we discovered a large variation in the sensitivity of the array that was uncorrected by the normal flat-fielding reductions. This effect has been traced to vignetting in the camera optics that has since been corrected. The most straightforward way of dealing with an illumination problem is to observe a point source at many places in the array and to map out the sensitivity variations from area to area. We were able to obtain these calibration observations for the K data, but for the J and H data we were forced to use a more indirect method. For the two shorter wavelengths, we compared 63 observations of 38 stars in our field that were previously measured by WS[2] with the published photometry from WS[2] and computed the difference between the published photometry and our observations as a function of position on the array. A quadratic correction function in the pixel coordinates was then defined and the six coefficients were adjusted to minimize the total error for more than 100 source extractions. By applying this correction function, the typical photometric nonrepeatability for multiple source observations was reduced from greater than 25% to less than 10%.

Exposure times per frame were set to give reasonable background photon statistics in the integration. With the 1.55 m telescope, however, sources brighter than ≈9.5, 8.5, and 8.0 mag in the J, H, and K bands, respectively, show saturation. We have applied a linear magnitude correction to these few bright objects to make their photometry agree with single-channel photometer results. A more detailed description of the reduction procedure will be published in a future paper (Young, Greene, & Lada 1993).

2.2. *SQIID–NOAO Observations*

Additional observations of the cluster and a large control field off the cluster were obtained in the period 1992 January 12–14 with the SQIID infrared array camera of NOAO attached to the 1.2 m telescope on Kitt Peak. SQIID consists of four 256 × 256 PtSi detector arrays mounted to permit simultaneous observations at four infrared bands: J, H, K, and L. For this experiment only data in the J, H, and K bands were obtained. The optics were configured to provide an imaging scale of 1.″3 pixel^{-1} at each wavelength. Five fields were observed toward the cluster. One field was roughly centered in the cluster and three others were obtained at the position of the star S Mon, and at positions 4′ east and 4′ west of S Mon. An additional cluster field toward the cone nebula was also imaged. Eight fields covering an area of roughly 225 arcmin^2 were imaged off the cluster in regions determined to be clear of molecular cloud material from examination of extensive CO surveys of the region (Blitz 1979) and the Palomar Sky Survey Prints. Six of these fields were observed roughly 45′ east of S Mon in a 3 × 2 mosaic grid with minimal (30″) overlap between the frames. Two additional control fields were observed 20′ and 30′ east of S Mon, respectively.

The integration time was 3 minutes for each observation in

each filter. Each SQIID field was observed at least twice with a 15″ positional offset or dither between each observation. The dithered observations were then combined using the IRAF data reduction package to yield images with effective integration times of 12 minutes for the six off fields in the 3 × 2 mosaic and 6 minutes for all the other fields on and off the cluster. In addition, as a further control, the same cluster field was observed on each of the three nights; however, observations taken on the different nights were not combined together. Flat fields for each color were constructed by median filtering and normalizing 20–30 (dark-subtracted) sky frames for each night's observations. Sky subtraction was performed by differencing a target frame and a sky frame. The sky frames were constructed from the filtered average of three sky observations which were usually obtained immediately before and after a target observation.

3. ANALYSIS

3.1. *Source Extraction and Photometry*

Source extraction and aperture photometry were performed on each image in each of our data sets using IRAF. For each image the routine DAOFIND (Stetson 1987) was used to extract stellar-like sources whose fluxes were significantly above the background. The single pixel threshold flux for extracting stars was set to 5 σ for both the SQIID and NICMOS images. Aperture photometry was performed on all the extracted sources in the SQIID and NICMOS data bases. For SQIID images, magnitudes were determined for each extracted star using an aperture 3 pixels in radius (i.e., 3.″9 on the sky). This corresponds to an aperture diameter which is twice that of the measured full width at half-power of a typical stellar point spread function in a SQIID image. Sky levels were also obtained around each star in an annulus whose inner radius was roughly 5″ and whose outer radius was 20″. Multi-aperture photometry was performed on a number of bright, well-isolated stars in the individual images and as well as on the photometric standards to determine the fraction of the total flux falling inside an aperture of 3 pixel radius. Typically, such an aperture was found to contain 90% of the stellar flux. The final instrumental magnitudes of the extracted SQIID stars were appropriately corrected to account for the missing flux. Comparison of the magnitudes derived for the SQIID cluster field observed from night to night indicated statistical (1 σ) photometric errors of 12% at J, and 7% at H and K for the SQIID observations.

The extensive overlapping of the NICMOS observations of the cluster enabled each star in that data base to be observed up to 4 times on different parts of the array. Aperture photometry was performed on all sources extracted from the individual NICMOS images. Magnitudes were determined for each star using an aperture of either 2 (J and H) or 4 (K) pixels in radius. This corresponds to an aperture radius of 3.″6 on the sky. Sky levels were also obtained around each star in an annulus whose inner radius was 5″ and whose outer radius was 10″. Although the individual images in the mosaic were not averaged together, the magnitudes derived for the stars in each overlapped region were combined in a noise-weighted average to obtain the final magnitudes for inclusion in our survey catalog. From comparison of the NICMOS and SQIID observations of roughly 138 stars observed in common in the cluster we estimate the following statistical (1 σ) photometric errors for the NICMOS observations: 15% at J, 12% at H, and 10% at K. In addition, the NICMOS observations were compared to previously published JHK photometry of 66 stars in the fields we imaged (WS[2], AS[2]). Neglecting the obviously saturated sources, we find reasonable agreement between the NICMOS data and the previously published photometry. The RMS differences between our data and the published results are 11%, 17%, and 11% in the J, H, and K bands, respectively.

3.2. *Absolute Photometric Calibration*

Photometric calibration for the SQIID data was established by the observations of bright standard stars taken from the list of Elias et al. (1982). The primary standard, HD 40335, was observed at several different elevations each night to derive airmass corrections for each color and establish the overall photometric scale. The derived J, H, and K magnitudes of HD 40335 corrected to zenith were found to agree to within 1% for the various elevations at which the star was observed. The overall photometric scale for the SQIID observations was established by adopting the J, H, and K fluxes for HD 40335 given by Elias et al. (1982). Redder secondary standards, GL 406 and GL 299, were also observed. Magnitudes for these stars were derived relative to HD 40335. Comparison of the colors derived for the secondary standards with those given by Elias et al. indicated that the SQIID colors for these stars were more consistent with the Johnson photometric system (Bessel & Brett 1988) than with the CIT system (Elias et al. 1982). We therefore did not apply any color corrections to the magnitudes we derived from our SQIID photometry and consequently, as a first approximation, we assume that the SQIID colors are in a photometric system very similar to that of Johnson 1966; see also Bessell & Brett 1988). However, we caution that our observations are not sufficient to derive meaningful color corrections to transform the SQIID observations to a standard photometric system.

The absolute photometric scale for the NICMOS observations was established by direct comparison with the calibrated SQIID observations of the cluster. One hundred and thirty-eight stars observed in common between the two data sets were used to establish the NICMOS absolute scale. When calibrated in this manner the NICMOS photometry agreed with previously existing JHK observations of 66 members of the cluster, well within the stated statistical errors.

3.3. *Astrometry*

The NGC 2264 field is sufficiently rich that there were many stars in the overlap regions. Such multiple observed stars were used to register the relative positions of the individual survey frames and to link all the frames into a single positional grid. Finally, the positional zero point, rotation angle, and scale of the grid were adjusted to minimize the errors when compared with the positions for the Walker stars measured by Lapicz (1984).

The quoted errors in the Lapicz positions are 0.″1 in each coordinate, and the RMS difference with our infrared positions is 0.″53 in each coordinate.

4. RESULTS

4.1. *Spatial Distribution*

As a result of our analysis of the NICMOS images of the cluster, we extracted 2091, 1835, and 1656 sources from the J, H, and K images, respectively. These sources ranged in apparent brightness between 7 and 17 mag at each wavelength,

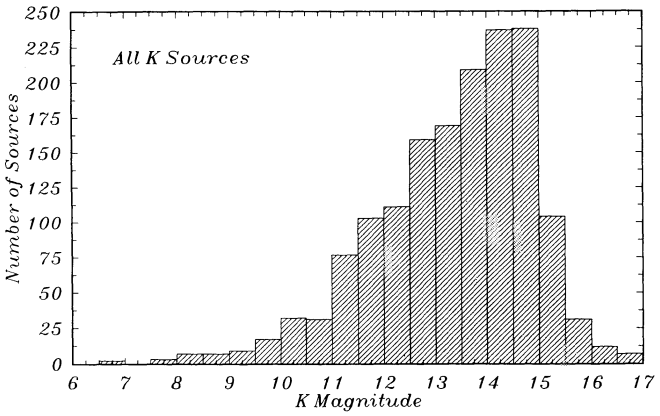

FIG. 2.—The K-band luminosity function (KLF) of all sources extracted from the NICMOS K-band survey of NGC 2264.

although the J images were somewhat deeper than the K images. Figure 1 (Plates 6 and 7) shows the positions and relative brightness of the sources extracted from the J-band survey alongside an image of the same region made at the same scale from a mosaic of I-band CCD images we have taken at the Steward Observatory 2.3 m telescope. The extent of the K survey is also indicated on the figure. The distribution of infrared sources is not uniform. The brighter J-band sources appear to be clustered into two groups: one around the bright star S Mon and the other somewhat to the north of the position of the cone nebula. Identical structure is observed in the H and K survey maps as well. This is in agreement with optical observations which also show the same two clusterings of stars in this region (Mathieu 1986). For the remainder of this paper we will be concerned only with those J, H, or K-band infrared sources which fall within the boundaries of the K-band survey.

4.2. *Luminosity Function*

Figure 2 displays the observed K luminosity function (KLF) of all the K-band sources we detected in the cluster with the NICMOS survey. The turnover in the luminosity function at a K magnitude of 15 is probably instrumental and suggests that the completeness limit of our survey is about 14.5 mag at 2.2 μm. Of the 1600 sources we detected we expect many to be background/foreground objects unrelated to NGC 2264. In order to estimate the number of infrared sources physically associated with the cluster requires knowledge of the number density of field sources in this region of the galaxy. In order to assess the extent of field source contamination we used the SQIID camera to obtain JHK observations of eight control fields located off the cluster. Altogether the area covered by the SQIID survey of the off fields was nearly half that covered by the NICMOS cluster survey. In Figure 3*a* we show the KLF for the sources in the eight control fields together with the luminosity function of the cluster. The luminosity function of the control fields in the plot has been scaled by a factor of 2.4 to account for the difference in surveyed areas between the cluster (540 arcmin^2) and the control fields (225 arcmin^2). The field star luminosity function turns over at a K magnitude of 14.5 indicating that these observations are complete to a K magnitude of about 14.0, roughly 0.5 mag brighter than the corresponding limit for the NICMOS survey of the cluster.

Comparison of the two luminosity functions shows that there is a clear excess of sources in the direction of the cluster for K magnitudes between 9.5 and 14.0. For sources with K magnitudes of 14.25 or less, we find an excess of 230 sources in the direction of the cluster. This corresponds to a 25% enhancement of the surface density of sources over that of the general field in this direction of the galaxy. These estimates of the size of the cluster population should be regarded as lower limits since we have not taken into account the effect of extinction due to dust in the associated molecular cloud which for the most part lies behind the cluster. Millimeter-wave spectral line observations of CO and NH_3 (Blitz 1979; Crutcher, Hartkof, & Giguere 1978; Margulis & Lada 1986; Krugel et al. 1987) show that the cluster lies projected onto a massive, dense molecular cloud core. The molecular gas is clumpy and we estimate the visual extinction to vary in a range of $\sim$2–15 mag through this region. The effect of extinction is to decrease the number of *background* field stars that would otherwise be

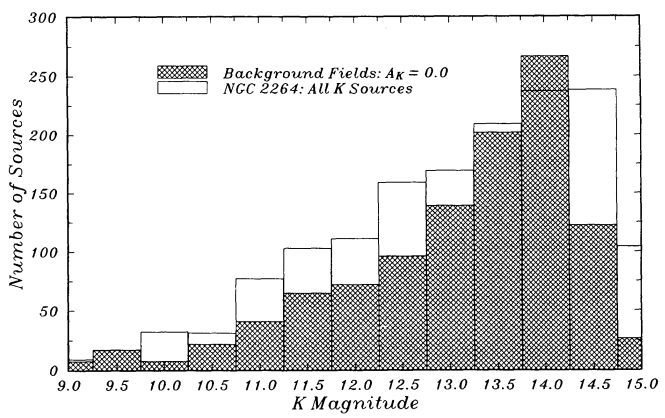

FIG. 3*a*

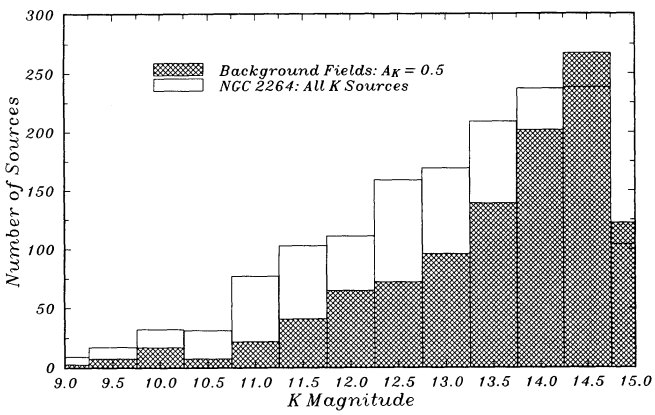

FIG. 3*b*

FIG. 3.—(*a*) The (K) luminosity function of sources observed toward NGC 2264 along with the corresponding luminosity function for the eight control fields observed off the cluster. The control field luminosity function has been scaled up by a factor of 2.4 to account for the difference in areas between the cluster and control fields. The control field luminosity function should be a good representation of the field star luminosity function in this direction of the galaxy. An excess of stars is clearly evident in the direction of the cluster for K magnitudes $\leq$13.5. (*b*) The K luminosity function of NGC 2264 along with the luminosity function of the scaled control fields which has been shifted by 0.5 mag to simulate the presence of extinction ($A_{vis} \approx 4.5$ mag) to the background field stars caused by the Mon OB 1 giant molecular cloud which lies behind the cluster. The difference between the two luminosity functions should be representative of the luminosity function of the cluster.

PLATE 6

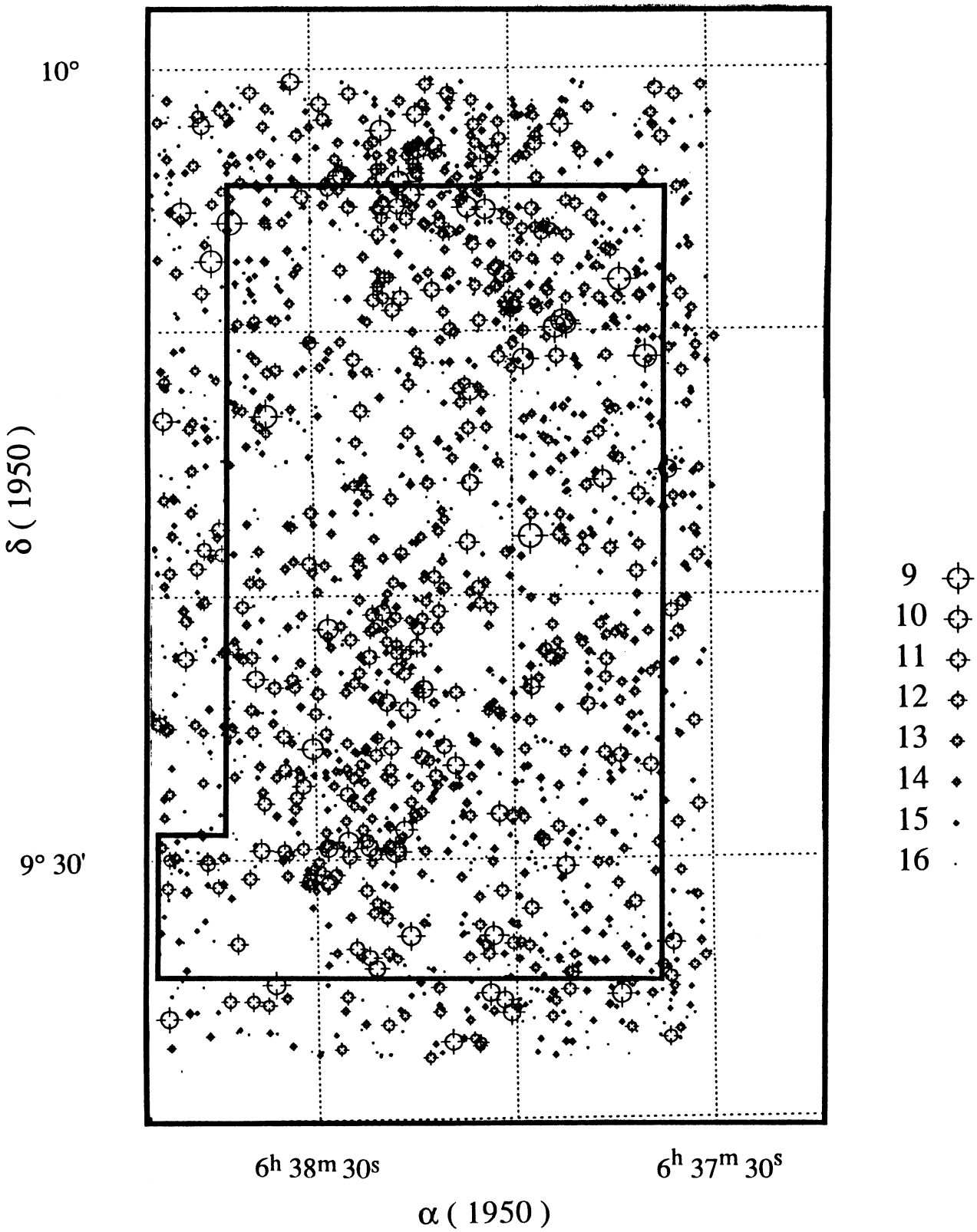

FIG. 1a

FIG. 1.—(*a*) Map of the distribution of all sources extracted in the *J*-band survey of NGC 2264 alongside (*b*) an *I*-band CCD mosaic of the same area and scale. The size of the symbol is proportional to the *J* magnitude of each individual source in the map. The largest symbol corresponds to a 9th mag star and the smallest to a 16th mag star. The inner box drawn on the *J* survey map indicates the extent of the *K*-band survey. The outer box exactly corresponds to the boundary of the *I*-band image.

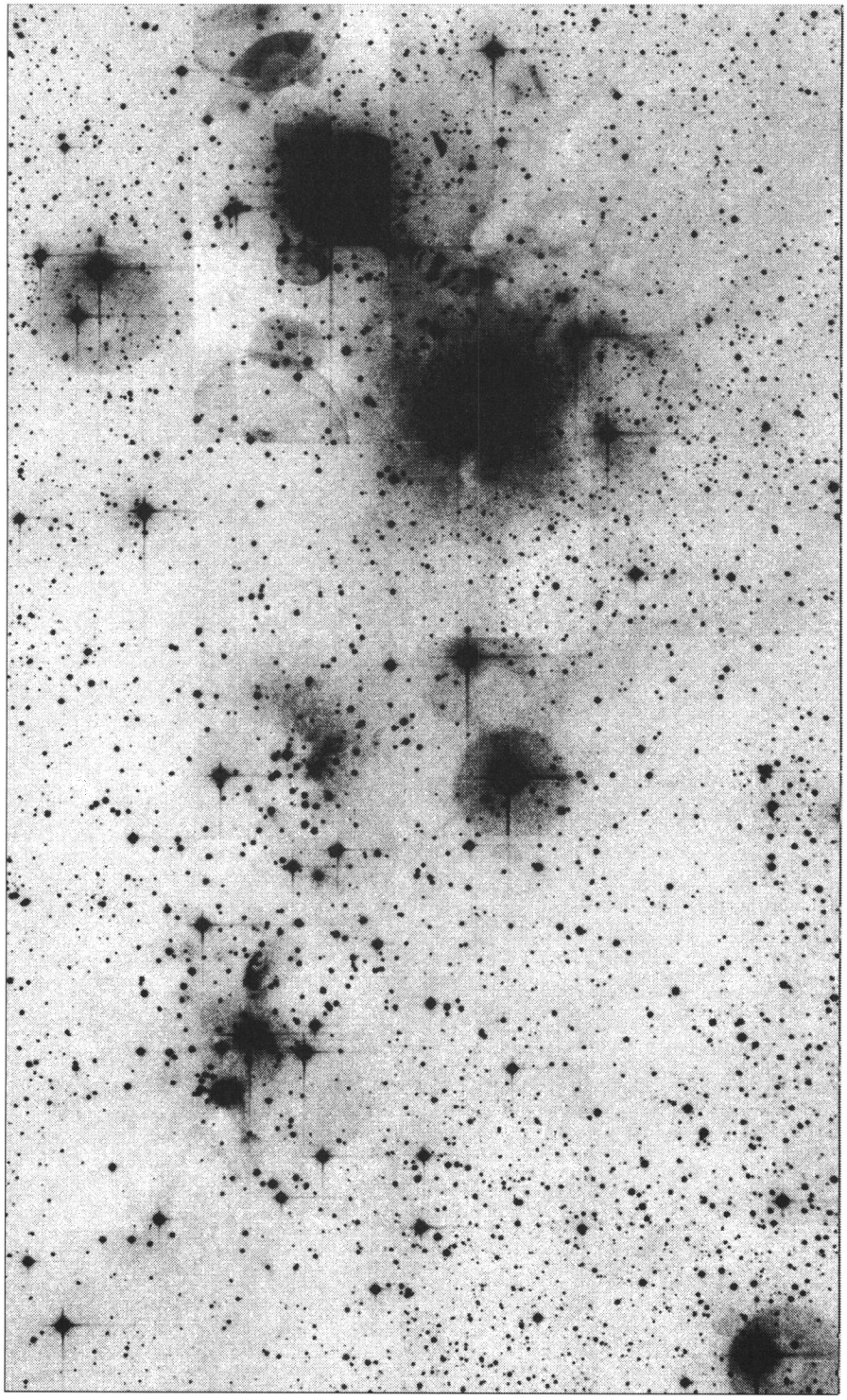

FIG. 1*b*

observed toward the cluster. To illustrate this effect quantitatively, we compare the cluster luminosity function to that of the control fields uniformly extincted by 0.5 mag at K (i.e., $A_v \approx 4.5$ mag) in Figure 3*b*. With the control field luminosity function adjusted in this manner, we find an excess of 485 sources brighter than 14.25 magnitudes at K in the direction of the cluster. This estimate of the size of the cluster population is likely an upper limit since we have probably overestimated the mean amount of extinction toward the cloud (see § 4.3 below). Our estimate of the size of the cluster population (360 ± 130 members) is roughly a factor of two lower than that (≈ 1100) derived for the cluster from optical observations by AS^2 after correcting for the difference in areas between the two surveys. The estimate of AS^2 was based on combining source counts from deep optical images and Walker's (1956) original observations. The origin of the difference between the two estimates is likely due to the fact that AS^2 made no attempt to correct for background/foreground field stars and in addition that the AS^2 survey was capable of detecting somewhat lower luminosity stars than our *JHK* survey.

Further examination of Figure 3*a* shows that at a K magnitude of 14 the number of observed sources in the cluster is less than that expected for field stars in this direction of the galaxy. This is not likely due to instrumental effects since 14th mag is above the completeness limit of our survey. The same is true at a K magnitude of 14.5 in Figure 3*b* where the field stars are extincted by 0.5 mag at K. This suggests that the luminosity function of the cluster flattens or turns over at low-K luminosities. A similar turnover is not apparent in the control field luminosity function. Indeed, for K magnitudes less than 14, the unextincted control field luminosity function is well modeled by a single power-law function whose index, determined from a least-squares fit, is 0.32 ± 0.03.

Figure 4*a* shows the KLF resulting from the subtraction of the luminosity functions of the cluster and extincted ($A_K = 0.5$ mag) control fields for K magnitudes between 9 and 14. This should represent the luminosity function for the cluster members. The luminosity function is observed to rise until a K magnitude of roughly 12.5 after which it begins to turn over. A linear, least-squares fit to the data between 9 and 12.5 mag gives a slope for the luminosity function of 0.32 ± 0.04 and is illustrated in Figure 3*a* (the similarity in the slopes of the control field and cluster luminosity functions is probably fortuitous). Figure 4*b* shows the corresponding *cumulative* luminosity function for the cluster sans field stars. The slope of the cumulative KLF in a log ΣN versus M_K plot is found to be 0.37 ± 0.03. The KLF of NGC 2264 compares very well to the cumulative KLFs recently derived for three similarly rich embedded clusters (NGC 2024, NGC 2068, and NGC 2071) in the Orion B (L1630) molecular cloud which have slopes in the range 0.37–0.38 (E. Lada et al. 1991). On the other hand, we note that the cumulative KLF recently determined for the rich OB cluster associated with M17 is characterized by a slope (0.26; C. Lada et al. 1991) which appears to be significantly smaller than that obtained for NGC 2264 (and the Orion clusters). Infrared luminosity functions have also been constructed for many young, but relatively poor clusters (i.e., clusters with less than 100 members; Lada & Lada 1991). In a recent study, Carpenter et al. (1993) constructed differential H band luminosity functions (HLFs) for 12 relatively distant poor clusters in the second and third quadrants of the galaxy. They found the average of the HLF slopes for this sample to be 0.37 ± 0.12, although the range in individual slope determinations was relatively wide (0.18–0.94). Greene & Young (1992) derived a slope of 0.17 ± 0.11 for the KLF of 80 suspected members of the Ophiuchi cluster, and DePoy et al. (1990) and Lada (1990) derived a slope of 0.21 ± 0.24 for the (cumulative) KLF of 21 members of the NGC 2023 cluster. However, because of the large statistical errors in these particular determinations (resulting from the small numbers of stars in most poor clusters), it is not possible to determine whether the observed variation in these slopes is physically meaningful (Carpenter et al. 1993). Moreover, it is not even clear whether any of these slopes is significantly different from that of either NGC 2264 or M17. Eiroa and Casali (1992) recently constructed a KLF for 51 members of an embedded cluster in the Serpens cloud, and, although they did not measure a slope of the cluster KLF, they did find evidence for a turnover at a K magnitude of approximately 13.5, similar to that observed for NGC 2264.

4.3. *Color-Color Diagram*

Of the infrared sources detected within the NICMOS K survey boundaries of the cluster, 1018 were detected in all three wavelength bands. Figure 5*a* shows the *JHK* color-color

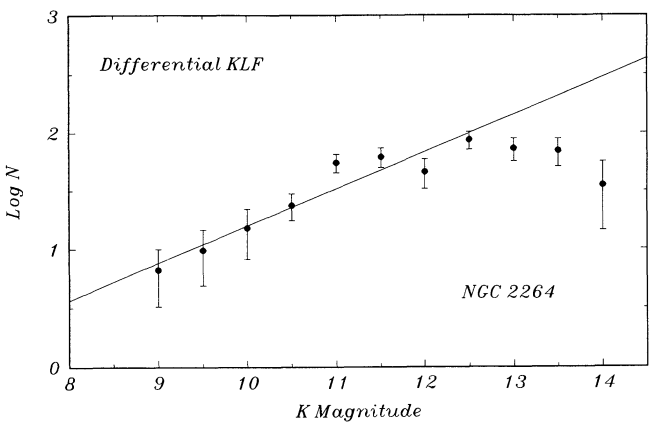

FIG. 4*a*

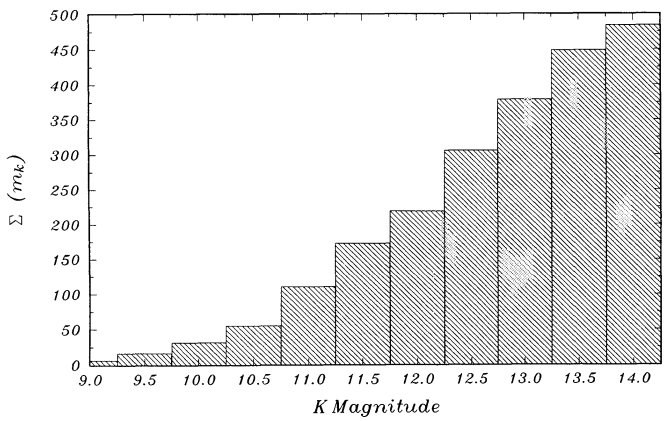

FIG. 4*b*

FIG. 4.—(*a*) The K luminosity function for the members of the NGC 2264 cluster. This luminosity function was constructed by differencing the luminosity functions of NGC 2264 and the scaled and extincted control fields (i.e., Fig. 3*b*). The straight line is a linear least-squares fit to the data between K magnitudes of 9 and 12.5. (*b*) The K luminosity function of the cluster plotted in cumulative form.

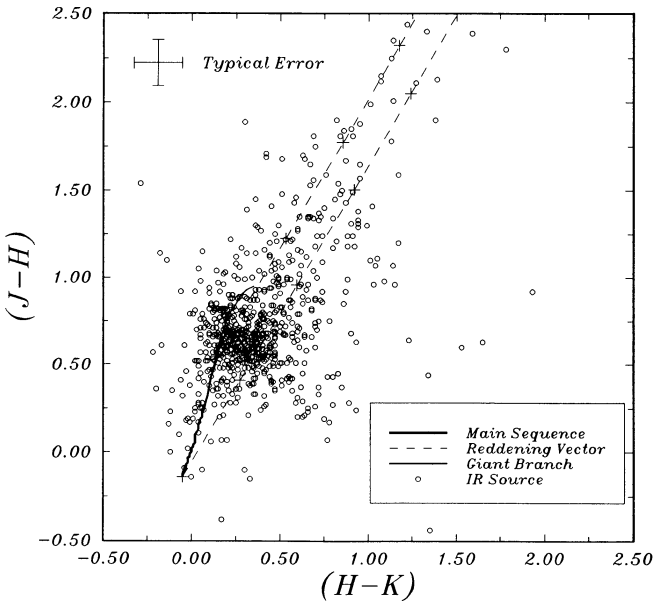

FIG. 5a

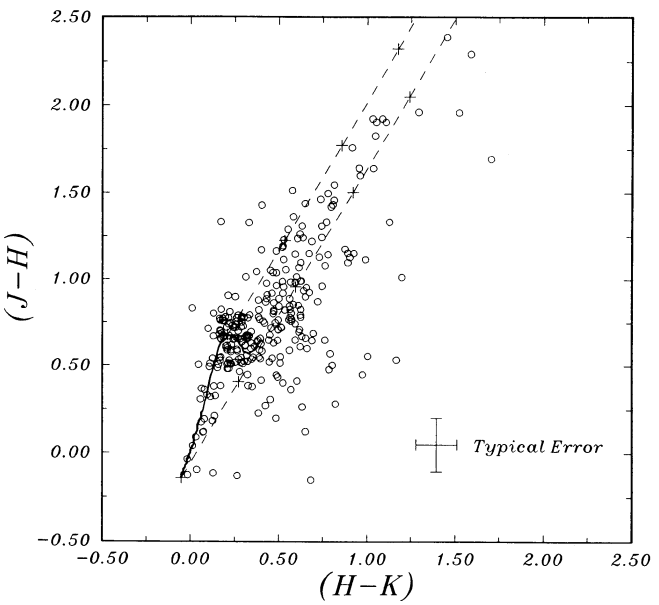

FIG. 5c

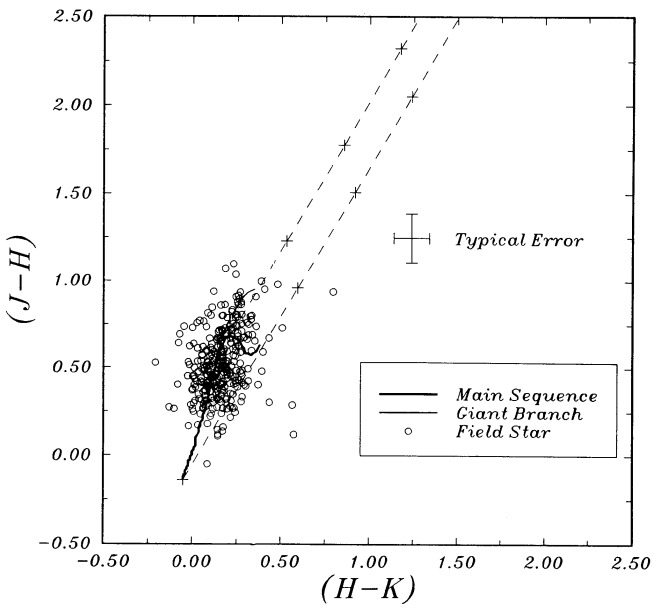

FIG. 5b

FIG. 5.—(*a*) The *JHK* color-color diagram for NGC 2264. All sources extracted from the NICMOS survey with magnitudes in the range 9.0–15.0 at *J* and *H* and 9.0–14.5 at *K* are plotted. In addition, we plot lines corresponding to the positions of main sequence and normal giant stars. The two parallel dashed lines are themselves parallel to the reddening vector which originates at the points where they intersect the main-sequence curve. These two lines form the reddening band or zone for main-sequence stars. Crosses are placed along these lines at intervals corresponding to 5 mag of *visual* extinction. Typical 1 σ error bars are also shown. (*b*) The *JHK* color-color diagram for the extracted stars in the eight SQIID control fields; otherwise, same as (*a*). (*c*) The *JHK* color-color diagram for four 5′ × 5′ SQIID fields in NGC 2264. Three of these fields are centered on S Mon and partially overlap with the northern boundary of the NICMOS *K* survey area. The fourth field is near the center of the cluster.

(hereafter CC) diagram for those (740) sources in the cluster that were brighter than our estimated completeness limits of 14.5 mag at *K* and 15.0 mag at *J* and *H*. Also plotted in Figure 5*a* is the locus of points corresponding to the position of the unreddened main sequence and the positions of red giant stars (Koornneef 1983). The two parallel dashed lines form the reddening zone or band for main-sequence stars; these lines are parallel to the reddening vector. Crosses are positioned along each reddening line at positions separated by a distance corresponding to 5 mag of visual extinction. Figure 5*b* shows the corresponding CC diagram for the 350 sources detected in all three bands in the control fields.

The CC diagram for the cluster is clearly different from that for the nearby control fields. The stars in the off fields are tightly clustered (within the errors) in a band around the main-sequence line and the giant branch while the cluster stars are considerably more scattered across the diagram. Most of the field stars fall in the region which corresponds to main-sequence spectral types between late G and late M (refer to Fig. 12 for the locations of various spectral types on the main sequence line). A smaller portion of stars are found around the giant branch. The majority of sources observed toward the cluster also fall on the main-sequence band, but it contrast to the control fields, are mostly found in the portion of the main sequence corresponding to M spectral types with relatively few in the portion corresponding to earlier spectral types. Unlike the control fields, a significant fraction of the stars in the direction of the cluster fall well outside the main sequence and giant bands. As can be seen in Figure 5*a*, these stars fall not only within but also outside the reddening band in the region forbidden for normal stellar photospheric colors (Lada & Adams 1992). As a check to ensure that the differences between the field and cluster CC diagrams are not due to an instrumental artifact resulting from the use of different imaging systems for the cluster and control field observations, we plot the CC diagram for four cluster fields observed with the SQIID camera in Figure 5*c*. The CC diagram constructed from the SQIID observations confirms the overall results of the NICMOS observations even though the area covered by the SQIID observations only partially overlaps the NICMOS *K* survey region.

Many of the differences between the cluster and field CC diagrams can be attributed to extinction caused by the molecular cloud behind the cluster. Extinction would affect the

observed distribution of field star colors in two ways. First, it would cause the fainter stars to be dimmed below the threshold of detection, particularly in the J-band images. For example, examination of the J-band luminosity function for JHK sources in the control fields indicates that a visual extinction of 4.5 mag would reduce the number of field stars which could be detected through the molecular cloud by a factor of 2! Second, the colors of the detected field stars would be displaced from their main-sequence values along the reddening vector and into the reddening band. The relative lack of main-sequence stars with colors corresponding to G–K spectral types in the cluster CC diagram suggests that the field stars in the direction of the cluster have been reddened by at least 2 mag of visual extinction and that most of the field stars are background objects rather than foreground stars. Furthermore, the dense clumping of sources with M star main-sequence colors in the cluster CC diagram suggests that majority of the background stars are reddened by about 2.4 mag of visual extinction by the molecular cloud. At the same time, however, the large number of stars that populate the reddening band in Figures 5*a* and 5*c* coupled with the large spread in their distribution within the band indicates that the extinction caused by the cloud is variable and can reach values as high as 15 mag at visual wavelengths for some stars.

Formally, if we ignore the photometric errors, more than 300 stars observed toward the cluster (Fig. 5*a*) have colors which place them outside the reddening band for main-sequence and giant stars. Photometric uncertainties can account for many but certainly not all of the stars observed outside the reddening band. For example, if we assume that all 740 JHK sources in the CC diagram have intrinsic colors which would place them in the center of the reddening band, then we would expect that random photometric errors would cause some fraction of the stars to fall outside the reddening band. Furthermore, we would expect as many stars to fall to the (lower) right of the reddening band, in the so-called infrared excess region (Lada & Adams 1992), as would fall to the (upper) left. However, we observe twice as many stars (234) in the infrared excess region to the right of the reddening band than in the forbidden region to the left (113). This asymmetry in the distribution of stars outside the reddening band suggests that there are roughly 120 stars in the cluster whose intrinsic colors are indicative of excess infrared emission. However, this is likely an underestimate of the number of stars in the infrared excess region, since contrary to our assumption above, the intrinsic colors of most normal stars place them not in the center but near the left boundary of the reddening band. As is evident in Figure 5 (see also Fig. 12), the distance of a normal star from the boundary of the reddening band depends on its spectral type. For example, early-type (OB) stars have intrinsic locations near the right boundary of the reddening band and late-type stars (G0–M0) have positions near the left boundary. Consequently, random photometric errors would place a higher fraction of early-type stars in the infrared excess region than later type stars. Conversely a higher fraction of late-type stars would be displaced to the left of the reddening band than to the right. Indeed, the right boundary of the reddening band is separated from the position of a K0 main-sequence star by a distance roughly corresponding to our 1 σ photometric errors. Since most stars in the cluster as well as the field are of relatively late spectral type, we would expect random photometric errors to introduce an asymmetry in the distribution of stars outside the reddening band which is opposite in sense to the one observed. Such effects on the distribution of stars in the cluster CC diagram can be approximately accounted for in a statistical sense by comparison of the cluster and control field observations. Indeed, in the control fields we find an asymmetry in the distribution of stars outside the reddening band which is reversed compared to that of the cluster, that is, in the control fields there are twice as many stars to the left of the reddening band as there are to the right, consistent with the fact that most of the field stars have late spectral types. Moreover, we find that the observed number of stars (116) which fall to the left of the reddening band in the control fields is consistent with the number (113) observed in the same region of the cluster CC diagram (after scaling for the difference in survey areas). However, the number of cluster stars (234) which fall to the right of the reddening band, considerably exceeds the number (65) expected from the field star statistics (see Fig. 5*b*). Thus, comparison of the cluster and field star CC diagrams indicates that roughly 170 stars observed toward the cluster have intrinsic colors suggestive of infrared excess emission.

In this regard, we note that based on $B-V$ and $V-K$ colors of a sample of 66 relatively bright stars from the list of Walker (1956), WS[2] found that roughly 30% of the stars in the sample exhibited excesses at wavelengths longer than 1 μm. Apparently, our JHK imaging observations of a significantly larger and more complete sample of cluster stars are consistent with the general conclusion of WS[2] that a significant fraction of stars observed toward the cluster have excess emission at near-infrared wavelengths.

4.4. *Color-Magnitude Diagram*

Figure 6 shows the K, $H-K$ color-magnitude (C-M) diagram for all the stars in the control fields. For reference, we also plot the locus of points corresponding to the main sequence for an apparent distance modulus of 9.7 mag, appropriate for NGC 2264 (Walker 1956). The field stars fall in a well-defined band parallel to the main-sequence line. This band is fairly well centered around a $H-K$ color corresponding to a mid- to late-K spectral type star, although the dispersion in observed $H-K$ color is large enough to include stars of a wider range of spectral types (i.e., A0–late M). We note that the CC diagram (Fig. 5*b*) suggests that most of the field stars have

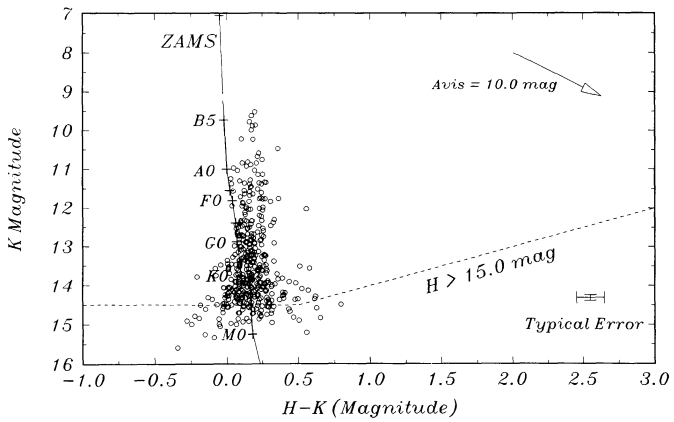

FIG. 6.—The K, $H-K$ color-magnitude diagram for the 417 HK sources in the control fields. The curve representing the ZAMS adjusted for the distance modulus of the cluster is plotted for reference. The dashed line represents the estimated completeness limits of the survey. The arrow represents the reddening vector corresponding to 10 visual mag of extinction.

G–K spectral types. The fact that the apparent K magnitudes of a large number of these stars in the C-M diagram are in the range (13.5–14.5) appropriate for K–M stars, indicates that these stars are more distant than NGC 2264. We estimate that the distance modulus to the typical dwarf field star is in the range of 10.5–11.0 mag.

Figure 7 shows the C-M diagram for all 1082 stars detected in both the NICMOS H and K bands toward the cluster. The distribution of stars in the cluster C-M diagram is considerably different from that of the stars in the control fields. The fundamental difference is that the scatter in $H-K$ color for the stars in the cluster fields is significantly greater than that of the field stars. The reddening vector is also plotted in the figure for a visual extinction of 10 mag. Given that the typical extinction through the molecular cloud is probably 2.5–4.5 mag, it is clear that extinction of the background field star population cannot be responsible for the large observed scatter. The scatter for most stars is likely to be intrinsic and due to excess infrared emission. This is evident from the locations of those JHK stars which were previously identified as being in the infrared excess region of the CC diagram. These stars have been plotted here as filled circles. For comparison, Figure 8 shows the C-M diagram for classical T Tauri stars (CTTSs) and weak-line T Tauri stars (WTTSs) observed in the Taurus dark clouds. WTTSs are low-mass PMS stars which do not display infrared excess emission while infrared excess is a defining characteristic of CTTSs. The segregation of excess and nonexcess sources and their overall distribution in the C-M diagram of NGC 2264 is similar to that of CTTSs in Taurus. This supports the contention that the increased scatter in the C-M diagram of the cluster compared to the field is a result of the presence in the cluster of sources with excess infrared emission. Moreover, the C-M diagram suggests that we may have underestimated the number of sources with infrared excess in NGC 2264 using the JHK CC diagram alone. For example, the majority of stars with $H-K \geq 1.0$ magnitude were not detected in the J-band images yet their large values of $H-K$ color make it unlikely that they are reddened field stars. Finally, it is interesting to note that CTTSs are thought to be low-mass stars, probably progenitors of stars similar to or less massive than the Sun.

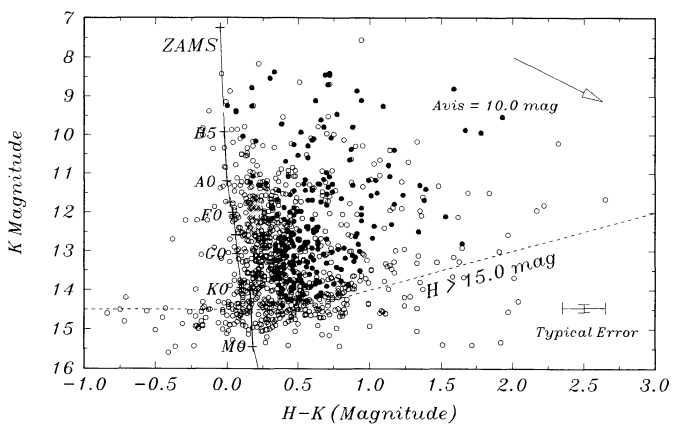

FIG. 7.—The color-magnitude diagram for all (1082) stars detected in both the H- and K-band surveys of the cluster. Filled circles represent those stars which have infrared excess emission. Otherwise, same as Fig. 6. As a result of reddening and excess infrared emission, the stars observed toward the cluster have a considerably larger dispersion in the color-magnitude diagram than the field stars observed in the nearby control fields.

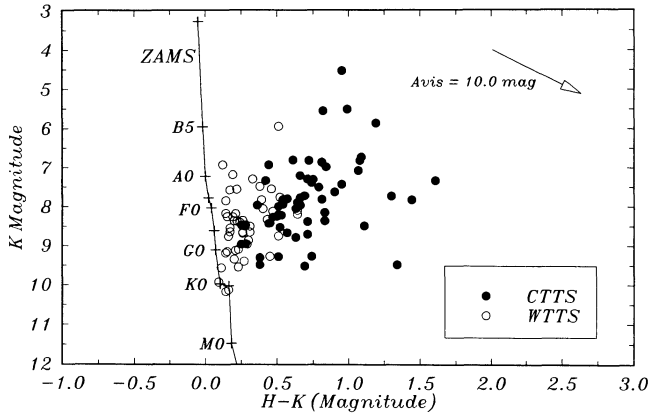

FIG. 8.—The color-magnitude diagram for classical T Tauri stars (CTTSs) and weak-line T Tauri stars (WTTSs) observed toward the Taurus-Auriga dark clouds. The data are taken from the compilation of Kenyon & Hartmann (1992). The ZAMS corresponding to the distance modulus of Taurus is also drawn for reference. Even though CTTSs are low mass stars, their brightness in the K band can, in some cases, be comparable to that of main-sequence A and B stars. This is largely due to infrared excess emission which is believed to originate in circumstellar disks.

Yet, as a result of infrared excesses, these stars can appear as bright as main-sequence A and B stars at 2.2 μm.

5. INTERPRETATION AND DISCUSSION

5.1. *The Cluster Luminosity Function*

In principle, the luminosity function of a very young cluster is closely related to its initial mass function. For a stellar system for which the mass function and mass-luminosity relation are power law in form [i.e., $dN(\log m_*) \propto m_*^{-\gamma} d \log m_*$; $L_K \propto m_*^{\beta}$], the slope of the K luminosity function can be shown to be

$$\alpha = \frac{\gamma}{2.5\beta}.$$

Here γ and β are the spectral indices of the stellar mass function and the K luminosity–stellar mass relation, respectively. For early-type (O–F) main-sequence stars which are sufficiently hot that their infrared emission is in the Rayleigh-Jeans regime, one can show that the K luminosity-mass relation is approximately a power law with $\beta = 2.0$ and consequently $\alpha = \gamma/5$ (e.g., Lada 1991). For an underlying mass function similar to that derived for local field stars by Salpeter (1955), $\gamma = 1.35$, and $\alpha = 0.26$. This is appears to be significantly different than the slope we derived for the KLF of NGC 2264: 0.32 ± 0.04. On the other hand, this is identical to the slope of the cumulative luminosity function of M17 derived by C. Lada et al. (1991) (we note that if the luminosity function of a stellar group is truly a single power law in form, the slopes of the differential and cumulative forms of the luminosity function are the same). The difference between M17 and NGC 2264 may not be surprising given that the stellar population of M17 is dominated by massive OB stars while that of NGC 2264 consists mainly of later type, low-mass stars. Indeed, the main-sequence K luminosity–mass relation for high-mass stars is known to be different than that of low-mass stars whose K-band emission is no longer on the Rayleigh-Jeans portion of the stellar spectrum. However, for the empirical mass-M_K relation constructed by Zinnecker, McCaughrean, & Wilking (1992), we derive $\beta = 3.1$ for main-sequence stars with G2–M6

spectral types, which would result in a decrease of the predicted slope of the KLF and increase the discrepancy with the observed KLF of NGC 2264. Moreover, it is well known that a single power-law shape is not consistent with the best estimates for the functional form of the field star IMF at all stellar masses. In particular, the field IMF appears to flatten or even turn over at masses below about 0.6 $M_\odot$ (e.g., Scalo 1978, 1986; Miller & Scalo 1979). For example, Scalo (1978) shows that if a lognormal function is fitted to the field star IMF, the slope of the IMF is variable and given by $\gamma = 0.94 + 0.94 \log (m_*)$. For a 1 $M_\odot$ star, which would be representative of the stellar populations in NGC 2264 (as well as the Orion B clusters), we expect $\gamma = 0.94$. For low-mass main-sequence stars, therefore, we predict $\alpha = 0.12$, which is clearly significantly less steep than observed for NGC 2264 (and the Orion B clusters).

Recently, E. Lada et al. (1991) suggested that the relatively steep slopes of the infrared luminosity functions of the Orion B clusters could be a result of the pre–main-sequence nature of the low-mass stars in these clusters. Low-mass PMS stars are more luminous for their mass than main-sequence stars while young higher mass stars will have luminosities close to their main-sequence values. This has the effect of increasing the proportion of low-luminosity to high-luminosity stars and should steepen the observed luminosity function of a young cluster. To test this hypothesis quantitatively requires knowledge of the mass-luminosity relation for pre–main-sequence stars, $\beta_{\rm pms}$. Recently, Simon et al. (1992) calculated the M_K-mass relation for 10^6 yr old PMS stars using published pre–main-sequence models. From their derived relation we find $\beta_{\rm pms} \approx 1.0$. With this value of β, appropriate for 10^6 yr old low-mass pre–main-sequence stars, we derive $\gamma = 0.80 \pm 0.10$ for NGC 2264, in good agreement with the predictions of the Miller-Scalo field star IMF at low stellar masses.

The nearly identical slopes derived for the cumulative luminosity functions of NGC 2071, NGC 2068, and NGC 2024 (E. Lada et al. 1991) further suggest that the mass functions of these clusters are similar to NGC 2264 and consistent with the local field star IMF. Evidently, any differences in either the ages of these clusters or in the natures of infrared stars within them are not clearly manifest in their cumulative K luminosity functions. The significantly different slope derived for the luminosity function of the M17 cluster is primarily a result of the fact that most of its (observed) members are OB stars whose luminosities are very close to main-sequence values, as would be expected for young massive stars.

The luminosity function of NGC 2264 also shows evidence for a flattening or turndown at relatively large K magnitudes. This apparent turnover in the luminosity function occurs at K magnitudes ($\approx$ 13.0–14.0) which at the distance of NGC 2264 (800 pc) corresponds to the brightness of a main-sequence star of early G spectral type (i.e., $M_* \approx 1\ M_\odot$) as well as the brightness of a 0.75 $M_\odot$ naked pre–main-sequence star of the same age as the cluster (5×10^6 yr).

This turnover appears to occur at a slightly higher mass than that (0.2 $M_\odot$) at which the local field star IMF is believed to peak (Scalo 1978). However, it is not clear how much significance to attach to this difference given the pre–main-sequence nature of the low-mass stars in cluster and the consequent uncertainties involved in converting observed K magnitudes to stellar masses. On the other hand, the K magnitudes at which the cluster luminosity function flattens and turns over correspond to masses roughly consistent with that (0.6 $M_\odot$, Scalo 1978) at which the local field star IMF begins to flatten out. Consequently, it appears that both the overall slope of the observed luminosity function at intermediate K magnitudes and its apparent turnover at relatively large K magnitudes are consistent with the assumption that the underlying cluster luminosity function is well described by the IMF for local field stars. This conclusion about the nature of the underlying IMF for NGC 2264 is consistent with that of AS[2] who derived an optical luminosity function for the cluster which was also well matched by the Miller-Scalo IMF. Finally, we do note that there is evidence of additional structure in the KLF. In particular, there is a small departure from the power-law fit between 11 and 11.5 mag, where there appears to be a small peak or spike in the luminosity function. Recently, Zinnecker et al. (1992) have pointed out that the onset of deuterium burning in contracting young stars can produce a spike in the luminosity function which does not correspond to a peak in the mass function of a young coeval cluster of naked pre–main-sequence stars. As the cluster evolves the position of this "deuterium burning" spike moves to fainter magnitudes (lower masses). For a cluster of the age of NGC 2264, however, the position of the deuterium burning peak is expected to have evolved beyond the location of the overall turnover we infer from Figures 3 and 4. However, if, as we argue below, star formation is not coeval in this cluster, then it may be possible that this feature is produced by deuterium burning in the more recently formed (i.e., 10^6 yr old) low-mass stars in the cluster.

5.2. *The Nature of the Infrared Excess Sources*

There are at least two possible origins for the anomalous colors of the 170 or so stars which likely possess infrared excess: (1) the presence of circumstellar material and (2) confusion from nearby or unresolved stellar companions. Confusion due to unresolved companions could give rise to such excess emission if the companions were very cold sources. Although it is reasonable to expect about half the stars in the cluster to have companions (Abt 1983), it is extremely unlikely that any more than a handful of stars could possibly have companions which are both unresolved and simultaneously at just the stage of early stellar evolution that they are cold enough to be nearly invisible at J band and at the same time dominate the emission at K band. Indeed, fewer than 10% of (very young) pre–main-sequence stars are known to contain infrared companions (Zinnecker & Wilking 1992). Therefore, in our opinion, it is very unlikely that the observed infrared excesses of the vast majority of the sources could be produced by confusion caused by unresolved or nearby companions.

Since early in their evolution most stars are associated with circumstellar gas and dust, infrared emission from such material could provide an appealing explanation for the existence of a large number of infrared excess sources in a young cluster like NGC 2264. As a first step to investigate the nature of the infrared excesses observed in NGC 2264, it is therefore useful to compare our observations with the JHK observations of those classes of young stellar objects which are well known to possess infrared excess emission arising from circumstellar material. Recently, Lada & Adams (1992) showed that Class I infrared (protostellar) sources, AeBe stars and the majority of T Tauri stars are characterized by JHK infrared colors which place them in the infrared excess region of the CC diagram. Comparison with the compilations of Lada & Adams indicates that the majority of excess sources in NGC 2264 have infrared colors which are not as red as protostars but more

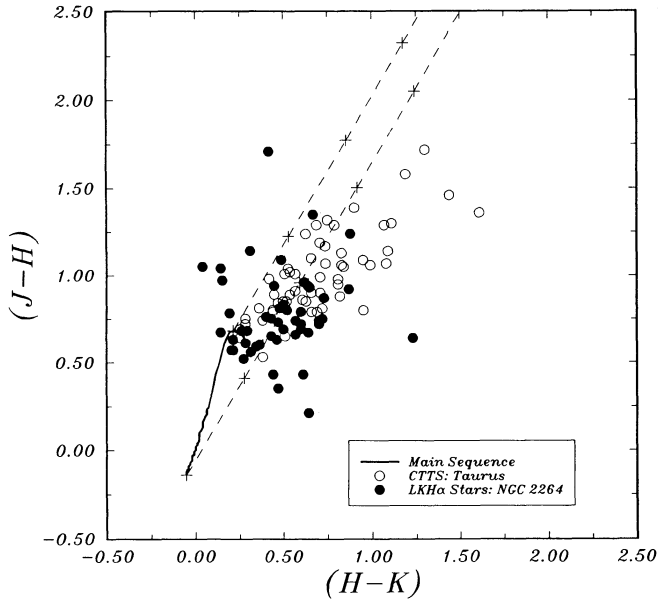

FIG. 9.—The color-color diagram for Hα emission-line stars originally identified in NGC 2264 by Herbig (1954) and detected in all three infrared bands in our survey. Plotted for comparison are the positions of the CTTSs in the Taurus-Auriga dark clouds. The positions of emission-line stars in NGC 2264 are slightly displaced from those of CTTSs in a manner consistent with the earlier spectral types and lower extinctions characteristic of the NGC 2264 emission-line population.

consistent with those of Class II sources: young emission-line stars such as T Tauri stars and AeBe stars. This is also evident in the comparisons of the *C-M* diagrams of NGC 2264 and CTTSs in Taurus as discussed earlier.

Forty years ago, Herbig (1954) conducted a survey for (Hα) emission-line stars in NGC 2264. At that time he detected 84 relatively bright stars with Hα line emission. More detailed spectrograms of a subset of these stars indicated that the great majority were late spectral type stars more similar to T Tauri stars than AeBe stars. Roughly 60 of the Herbig emission-line stars fall within our *K* survey area. In Figure 9 we plot the *JHK* color-color diagram for 48 Hα sources which we were able to unambiguously detect in the three infrared bands. Half of these stars fall in the infrared excess region of the *JHK* color-color diagram. For comparison we also plot the positions of CTTSs in the Taurus dark clouds. Similar to the emission line stars in NGC 2264, about half the CTTSs in Taurus fall in the infrared excess region of the *JHK* CC diagram. However, although there is some degree of overlap, these two populations of emission-line stars appear to be segregated on the CC diagram. The NGC 2264 emission-line stars appear to be diagonally offset below the CTTSs in a manner consistent with either a difference in mean extinctions to the two groups of about 2.5 visual mag or a difference in the mean spectral types of the stars themselves or a combination of both. In this regard, we point out that the spectral types of the emission-line stars in NGC 2264 generally range from G to K while those for the CTTSs in Taurus range between K and M (Herbig 1954; Walker 1972; Herbig & Bell 1988). Otherwise, the nature of two groups of stars appears very similar. In particular, even though the Lick Hα stars in NGC 2264 are systematically earlier in spectral type than their counterparts in Taurus, they are not systematically more luminous in the infrared. Apparently, the emission-line survey of Herbig selected earlier type stars in the more distant NGC 2264 region than are observed in the nearby Taurus clouds. The fact that emission-line stars in NGC 2264 are not systematically brighter than CTTSs is most likely a result of the age difference between the two stellar groups. NGC 2264 is roughly 5 times as old as the Taurus T Association. Therefore, for a given mass star, YSOs in NGC 2264 should be less luminous than YSOs in the Taurus dark clouds.

The known Hα stars only account for a little more than 15% of the infrared excess (hereafter IREX) stars in the cluster. Comparison of the positions of CTTSs in Figure 9 with the locations of the entire sample of infrared stars observed toward NGC 2264 in Figure 5*a* indicates that there is a significant population of cluster IREX stars which overlaps the region where CTTSs are found. However, similar to the case for the known Hα-emitting stars, large concentrations of cluster IREX stars are also located more or less diagonally below the positions where the CTTSs in Taurus are found. This is clearly illustrated in Figure 10 which compares the frequency distribution of $(J-H)$ colors for those cluster stars which we find in the excess region of the CC diagram with the frequency distribution of $(J-H)$ colors for CTTS. Clearly most of the excess stars in the cluster have $J-H$ colors that are bluer than observed for CTTSs. It is useful to divide the IREX stars in NGC 2264 into two populations: red IR excess stars whose $J-H$ colors are greater than 0.6 mag and blue IR excess stars whose $J-H$ colors are less than 0.6 mag. There are roughly equal numbers of excess stars in each population. Figure 11 shows the *K*-band luminosity functions for the entire population of excess sources, the red IREX sources and CTTSs adjusted to the distance of NGC 2264. The luminosity function for red IREX sources is similar to that of the CTTSs in its centroid and overall extent. Apparently, there is a significant population of excess stars in NGC 2264 which have similar infrared colors ($J-H$ as well as $H-K$) and infrared luminosities as CTTSs in Taurus. This is also clear in the comparisons of the *C-M* diagrams for the cluster and the CTTSs. Indeed, given that only half of the CTTs themselves fall in the infrared excess region of the CC diagram, there are roughly twice as many stars with apparent CTTS characteristics in NGC 2264 as there are in the Taurus sample. On the other hand, the luminosity function of the blue IREX sources is clearly skewed toward faint magnitudes compared to that of the CTTSs. These sources appear to constitute a population

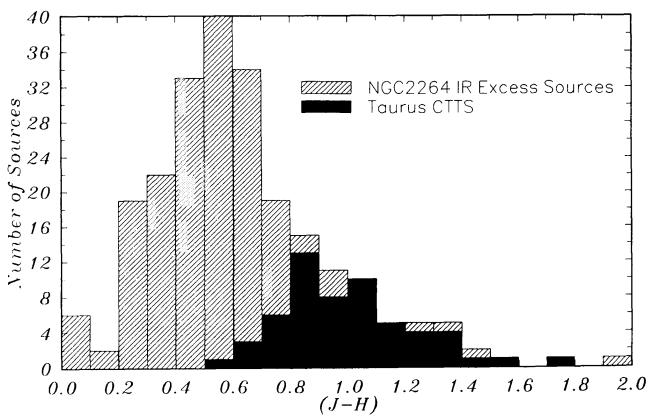

FIG. 10.—Frequency distribution of $(J-H)$ colors for infrared excess sources in NGC 2264 and CTTS in Taurus.

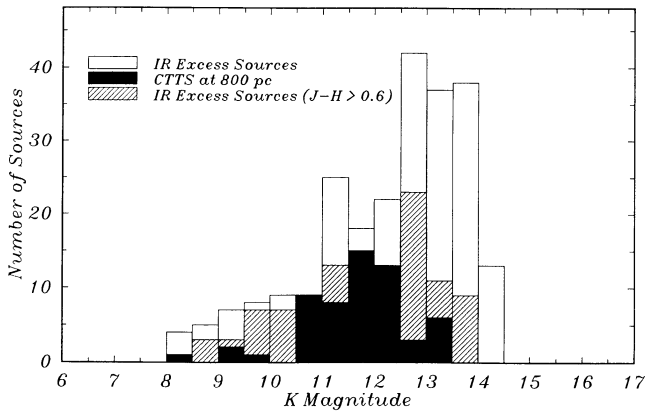

FIG. 11.—Comparison of the K luminosity functions for infrared excess sources in NGC 2264 and CTTSs in Taurus. The luminosity function for NGC 2264 excess sources with $J-H$ colors ≥ 0.6 mag is also shown. See text for discussion.

distinct in its infrared colors and luminosities from those of CTTSs.

During the last few years numerous observational and theoretical studies have suggested that circumstellar disks are responsible for the observed infrared excesses around T Tauri stars (e.g., Lynden-Bell & Pringle 1974; Rucinski 1985; Beall 1987; Adams, Lada, & Shu 1987, 1988; Kenyon & Hartmann 1987; Beckwith et al. 1990; Bertout & Basri 1991, etc.). Indeed, Lada & Adams (1992) showed that the distribution of CTTSs in the JHK color-color diagram was well matched by the distribution of JHK colors produced by a range of standard circumstellar disk models. In particular, the positions of most CTTSs in the infrared excess region could be explained by circumstellar disk models with relatively cool (i.e., $T_{\rm eff} \approx 3000$ K) central stars and modest amounts of extinction (i.e., $A_v \approx$ 1–3 mag) consistent with optical estimates of spectral types and extinctions to these stars. Such models could also match the colors of the red IREX stars in NGC 2264. However, these models are not unique in the sense that circumstellar disks with hotter ($T_{\rm eff} \approx 4000$–6000 K) central stars can equally well match the NGC 2264 observations, provided the extinction to the stars can reach large values (5–15 visual mag). To distinguish between these two possibilities would require an independent determination of the extinction to these stars. In any event, we conclude that the red IREX stars can be modeled as a population of late-type YSOs with circumstellar disks. However, whether these YSOs constitute a population similar in nature to CTTSs (i.e., K–M stars) or to more heavily reddened slightly earlier type (i.e., F–K) stars cannot be ascertained from the infrared data alone. In either case, however, it is clear from comparison with the models that significant amounts of extinction are required to explain the positions of red IREX stars on the CC diagram. This is in contrast to the observations of the B stars in the cluster (see Fig. 9) for which Walker (1956) derived a small and uniform amount of reddening: 0.082 mag in $B-V$ corresponding to roughly 0.25 visual mag. Our observations clearly suggest that extinction is not uniform for all cluster members. This is consistent with *IRAS* observations which indicate that active star formation is occurring within the molecular cloud behind the cluster (Margulis et al. 1989). It is likely, therefore, that the red IREX stars represent a population of YSOs which are partially buried within the cloud and as a result have appreciable extinctions. It is not clear whether such stars represent an extension of the cluster into the molecular cloud or a separate population of YSOs formed at a more recent epoch in the background cloud. In any event, given their similarity in JHK colors and luminosities to CTTSs, some of these stars are likely to have ages which are also typical of CTTSs (i.e., $\approx 10^6$ yr). This suggests that the duration of star formation in the cluster has been roughly 4–5 $\times$ 10^6 yr. Evidently, star formation in NGC 2264 is *not* coeval on time scales less than the age of the cluster.

In Figure 12 we compare the JHK CC diagram for circumstellar disk models with that of the infrared excess stars in the cluster. We plot four grids of circumstellar disk models taken from Lada & Adams (1992). The first three models represent circumstellar disk systems around earlier type central stars which have surface temperatures of 5000, 6000, and 10,000 K corresponding roughly to early K, G, and A stars, respectively. Each grid consists of 18 separate disk models each of which generates 10% of the total intrinsic luminosity of the star + disk system. The models in each grid are characterized by six different line-of-sight inclinations and three different power-law disk temperature gradients as described by Lada & Adams (1992). The models for central stars with 5000–6000 K central temperatures overlap with a significant number of blue IREX stars near the tip of the main sequence. This comparison suggests that this group of blue IREX stars in the cluster can be explained as relatively unextincted YSOs with circumstellar disks and central stars of earlier spectral type (G–K) than typical for CTTSs. The fact that these objects appear to have very little extinction implies that they are foreground to the molecular cloud, similar to the B stars in the cluster. The majority of these blue IREX sources have K luminosities which are similar to main-sequence stars with F–K spectral types. For the luminosities of these IREX stars to be consistent with pre–main-sequence evolutionary tracks, the stars must have ages of 5 $\times$ 10^6 yr or greater which is consistent with the ages of the more massive members of the cluster derived from optical observations. Thus it is possible that these objects are a population of low-mass pre–main-sequence stars which formed at the same time and in roughly the same place as the visible main-sequence B stars in the cluster. Of course, it is also possible that some of these stars are objects with normal colors which appear as excess stars in our data due to the measurement uncertainties in their photometric magnitudes. Based on the statistical grounds discussed earlier, we would expect about half of these stars to be normal (mostly background) stars without intrinsic infrared excess. Finally we note that there are roughly 30 blue IREX sources which have $H-K$ colors larger than can be accounted for by the standard disk models. These stars are also displaced from the main sequence by an amount (i.e., $\geq 2\ \sigma$) greater than that which can be easily accounted for by the uncertainties in our photometric measurements and moreover are observed independently in both the SQIID and NICMOS data sets. These stars occupy a region of the CC diagram which could be populated by AeBe stars which are surrounded by disks with central holes (Lada & Adams 1992). This is illustrated in Figure 12 where we plot for comparison one grid of models which represents an AeBe star surrounded by a disk with a central hole. However, only a handful of stars in this region of the CC diagram have magnitudes consistent with A or B stars, and it seems unlikely that disk models even with holes can explain their unusual colors. If these objects were indeed systems with hot central stars and annular disks, they would fall well below the main sequence on the H-R

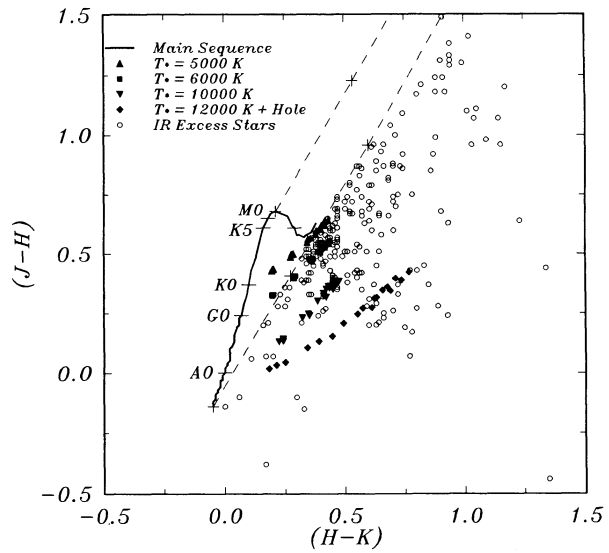

FIG. 12.—Color-color diagram for infrared excess sources in NGC 2264. Plotted for comparison are the locations of (unreddened) standard disk models for stars of varying central temperature with corrections for realistic stellar opacities as described by Lada & Adams (1992). The four sets of disk models shown here represent essentially passive disks with only 10% of the total system luminosity intrinsic to the disk. For each central star, a model grid consists of 18 models corresponding to disks of six different line-of-sight inclinations (cos θ = 1.00, 0.866, 0.707, 0.50, 0.25, and 0.10) for each of three different temperature gradients in the disk. The model disk associated with the 12,000 K central star contains a central hole with an inner disk temperature of 2,000 K. With various amounts of reddening the colors of most of the excess sources in NGC 2264 can be fit by such disk models.

diagram. For these stars we cannot ascertain the origin of their excesses with the currently available data.

In summary, the infrared excess sources of NGC 2264 are very similar in their near-infrared colors to young emission-line stars such as T Tauri and Herbig AeBe stars. Circumstellar disk models can account for the colors of most of these sources. Only a few *JHK* sources have large excess and lie far enough up the reddening line to be Class I sources and protostellar candidates. Therefore, our observations suggest that as many as half of the cluster members (i.e., 170 of 360) may be Class II YSOs surrounded by circumstellar disks. Indeed, it is likely that this estimate is a lower limit since stars with circumstellar disks and spectral types between K0 and M5 are just as likely to appear in the reddening band as in the infrared excess region. This is apparent both from both model predictions (Fig. 12) and the observation (Fig. 9) that roughly only half the known CTTSs in Taurus as well as half the Hα stars in NGC 2264 fall within the reddening band of the *JHK* CC diagram. This suggests that the vast majority of stars in the cluster have circumstellar disks which in turn suggests that the dispersal time for such disks is at least as long as the age of the cluster or 5×10^6 yr. In addition, many of the infrared excess stars are characterized by appreciable amounts of reddening suggesting that the cluster extends into the molecular cloud where star formation may still be proceeding.

6. SUMMARY AND CONCLUSIONS

We have presented the first detailed results of our infrared imaging survey of the young cluster NGC 2264 and nearby control fields. As a result of our survey we have been able to enlarge the sample of cluster stars with measured *JHK* magnitudes by more than an order of magnitude. By comparison of this data base with extensive *JHK* observations of field stars from nearby control fields we have been able to obtain quantitative estimates of the size of the cluster population, its luminosity function, and the number of members with excess infrared emission and circumstellar disks. These new findings significantly extend and at the same time largely corroborate the results of earlier infrared and optical studies of this cluster (e.g., WS[2], AS[2], and Margulis et al. 1989). The main conclusions resulting from our analysis of these observations are summarized as follows:

1. Extensive observations of control fields near NGC 2264 indicate that most of the stars observed in the direction of the cluster are background field stars. Within the region completely surveyed at 2.2 μm (*K* band), we estimate that there are 360 ± 130 sources which are members of the cluster. The uncertainty in our estimate of the size of the cluster population is almost entirely due to the uncertainty in the extinction to the background field star population which results from the presence of a dense molecular cloud behind the cluster.

2. The slope of the *K* luminosity function (KLF) of the cluster is found to be significantly steeper at intermediate magnitudes than that expected for a population of young main-sequence stars. However, it is similar to the slopes derived for the KLFs of NGC 2024, NGC 2071, and NGC 2068, three young embedded clusters in the Orion B molecular cloud. In addition, the KLF for NGC 2264 appears to flatten or even turn over at *K* magnitudes corresponding to the brightness expected for an unreddened 0.75 $M_\odot$ pre–main-sequence star at the distance of the cluster. With the adoption of a mass-luminosity relation appropriate for young (10^6 yr old) pre–main-sequence stars (Simon et al. 1992), we find that both the overall slope of the cluster KLF at intermediate magnitudes and the turnover at relatively large magnitudes are well modeled by an underlying mass function which is very similar in form to the IMF of the local field star population derived by Scalo (1978, 1986).

3. From analysis of the *JHK* colors of 740 stars observed toward the cluster we find that roughly 170 have colors indicative of intrinsic excess infrared emission. Consequently, a relatively large fraction ($50\% \pm 20\%$) of the cluster members appear to be infrared excess stars. These stars have near-infrared colors similar to those of young emission-line stars such as classical T Tauri stars and Herbig AeBe stars. Circumstellar disk models can account for the colors of most of these sources. Many of these stars are characterized by relatively large amounts of extinction and may be partially embedded in the molecular cloud behind the cluster where star formation activity is still occurring. Consequently, the duration of star formation in this cluster (i.e., $4\text{–}5 \times 10^6$ yr) appears comparable to its age. The fact that a very large fraction of the cluster members are inferred to have circumstellar disks also suggests that the dispersal time for such disks is at least as long as the age of the cluster, that is, $\geq 5 \times 10^6$ yr.

We thank Marcia and George Rieke for making available the NICMOS camera used for this project. The NICMOS camera is supported by NASA grant NAGW-2606. We gratefully acknowledge the efforts of Marika Roberson in assisting us with the formidable task of reducing the hundreds of infrared images generated by this survey. We thank Barry Rice for his efforts in assisting us with determining difficult flat-field

corrections for our NICMOS observations. We are grateful to Elizabeth Lada for critical assistance in both obtaining and reducing the SQIID observations. We thank Richard Elston for acquiring the pilot observations for this study. T. P. G. acknowledges support from a National Research Council–Ames Research Center Research Associateship for part of this work. This study was largely supported by NSF grant AST 8815753 awarded to the University of Arizona.

REFERENCES

Abt, H. A. 1983, ARA&A, 21, 343
Adams, F. C., Lada, C. J., & Shu, F. H. 1987, ApJ, 321, 788
———. 1988, ApJ, 326, 865
Adams, M. T., Strom, K. M., & Strom, S. E. 1983, ApJS, 53, 893 (AS^2)
Barsony, M., Shombert, J. M., & Kis Halas, K. 1991, ApJ, 379, 221
Beall, J. H. 1987, ApJ, 316, 227
Beckwith, S. V. W., Sargent, A. I., Chini, R. S., & Gusten, R. 1990, AJ, 99, 924
Bertout, C., & Basri, G. 1991, in The Physics of Star Formation and Early Stellar Evolution, ed. C. J. Lada & N. D. Kylafis (Dordrecht: Kluwer), 649
Bessell, M. S., & Brett, J. M. 1988, PASP, 100, 1134
Blitz, L. 1979, Ph.D. thesis, Columbia Univ.
Carpenter, J., Snell, R. L., Schloerb, P. F., & Skrutskie, M. F. 1993, ApJ, in press
Crutcher, R. M., Hartkopf, W. I., & Giguere, P. T. 1978, ApJ, 226, 839
DePoy, D. L., Lada, E. A., Gatley, I., & Probst, R. 1990, ApJ, 356, L55
Eiroa, C., & Casali, M. M. 1992, A&A, 262, 468
Elias, J. H., Frogel, J. A., Matthews, K., & Neugebauer, G. 1982, AJ, 87, 1029
Gatley, I., Merrill, K. M., Fowler, A. M., & Tamura, M. 1991, in Astrophysics with Infrared Arrays, ed. R. Elstau (ASP Conf. Ser., 14), 230
Greene, T. P., & Young, E. T. 1992, ApJ, 395, 516
Herbig, G. H. 1954, ApJ, 119, 483
Herbig, G. H., & Bell, R. 1988, Lick Obs. Bull., 1111
Johnson, H. L. 1966, ARA&A, 4, 193
Kenyon, S. J., & Hartmann, L. W. 1987, ApJ, 323, 714
———. 1992, unpublished observations
Koornneef, J. 1983, A&A, 128, 84
Krugel, E., Gusten, R., Schulz, A., & Thum, C. 1987, A&A, 185, 283
Lada, C. J. 1991, in The Physics of Star Formation and Early Stellar Evolution, ed. C. J. Lada & N. D. Kylafis (Dordrecht: Kluwer), 329
Lada, C. J., & Adams, F. C. 1992, ApJ, 393, 278
Lada, C. J., DePoy, D. L., Merrill, M., & Gatley, I. 1991, ApJ, 374, 533
Lada, C. J., & Lada, E. A. 1991, in The Formation and Evolution of Star Clusters, ed. K. Janes (ASP Conf. Ser., 13), 3
Lada, E. A. 1990, Ph.D. thesis, Univ. of Texas
Lada, E. A., DePoy, D. L., Evans, N. J., & Gatley, I. 1991, ApJ, 371, 171
Lapicz, D. 1984, PASP, 96, 437
Lynden-Bell, D., & Pringle, J. 1974, MNRAS, 168, 603
Margulis, M., & Lada, C. J. 1986, ApJ, 309, L87
Margulis, M., Lada, C. J., & Snell, R. N. 1988, ApJ, 333, 316
Margulis, M., Lada, C. J., & Young, E. T. 1989, ApJ, 345, 906 (MLY)
Mathieu, R. 1986, Highlights Astron., 7, 481
Miller, G. E., & Scalo, J. M. 1979, ApJS, 41, 513
Rieke, M. J., Montgomery, E. F., Rieke, G. H., Vural, K., Blessinger, M., & Kleinhans, W. 1989, in Proc. of the Third Infrared Detector Workshop, ed. C. R. McCreight (NASA Tec. Mem. 102209), 321
Rucinski, S. M. 1985, AJ, 90, 2321
Salpeter, E. E. 1955, ApJ, 121, 161
Scalo, J. M. 1978, in Protostars and Planets, ed. T. Gehrels (Tucson: Univ. of Arizona Press), 265
———. 1986, Fund. Cosmic Phys., 11, 1
Simon, M., Chen, W. P., Howell, R. R., Benson, J. A., & Slowik, D. 1992, ApJ, 384, 212
Stetson, P. B. 1987, PASP, 99, 191
Strom, S. E., Strom, K. M., & Yost, J. 1971, ApJ, 165, 479
Walker, M. F. 1956, ApJS, 2, 365
———. 1972, ApJ, 175, 89
Warner, J. W., Strom, S. E., & Strom, K. M. 1977, ApJ, 213, 247 (WS^2)
Young, E. T., Greene, T. P., & Lada, C. J. 1993, in preparation
Zinnecker, H., McCaughrean, M., & Wilking, B. A. 1992, in Protostars and Planets III, ed. G. Levy & J. Lunine (Tucson: Univ. of Arizona Press), in press
Zinnecker, H., & Wilking, B. A. 1992, in Binary Stars as Tracers of Stellar Formation, ed. A. Duquennoy & M. Mayor (Cambridge: Cambridge Univ. Press), in press